Journal of Applied Fluid Mechanics, Vol. 12, No. 3, pp. 715-728, 2019.
Available online at www.jafmonline.net, ISSN 1735-3572, EISSN 1735-3645.
DOI: 10.29252/jafm.12.03.28836

Turbulent Energy Dissipation Rate and Turbulence Scales in the Blade Region of a Self-Aspirating Disk Impeller

J. Stelmach†, R. Musoski, C. Kuncewicz and M. Głogowski

Lodz University of Technology, Faculty of Process and Environmental Engineering
Wolczanska 213, 90-924 Lodz, Poland

†*Corresponding Author Email: jacek.stelmach@p.lodz.pl*

(Received January 29, 2018; accepted December 19, 2018)

ABSTRACT

Instantaneous radial and axial velocitieques of water in the tank with a self-aspirating disk impeller operating without gas dispersion were measured by the PIV method. A comparison of mean square velocity pulsations confirmed previous observations that the area in which turbulence is non-isotropic is small and extends about 3 mm above and under the impeller and radially 12,5 mm from the impeller blade tip. Based on velocity measurements, the distributions of energy dissipation rates were determined using the dimensional equation $\varepsilon = C \cdot u'^3/D$ and Smagorinsky model. Adoption of the results of the dimensional equation as a reference value allowed us to determine the Smagorinsky constant value. This value appeared to be smaller than the values given in the literature. It has been shown that eddies in a small space near the impeller had sufficient energy to break up gas bubbles flowing out of the impeller. Based on the obtained energy dissipation rate distributions, appropriate turbulence scales were determined.

Keywords: Energy dissipation rate; Turbulence scales; Self-aspirating disk impeller.

NOMENCLATURE

B	baffle width
D	impeller diameter
d	diameter of gas bubble or eddy
E	energy
g	acceleration of gravity
H	liquid height in the tank
h	distance of the impeller from the tank bottom
k	turbulent kinetic energy per unit mass
k	wave number
N	rotational frequency
T	tank diameter
u'	mean square velocity pulsation (in terms of RMS)
ε	energy dissipation rate
η_K	spatial Kolmogorov scale
Λ	spatial integral scale
λ	spatial Taylor scale
ρ	density
σ	surface tension
Re	Reynolds number
Fr'	modified Froude number

1. INTRODUCTION

Liquid circulation in the tank with a self-aspirating disk impeller has an influence on the residence time of gas in the tank (Kurasiński and Kuncewicz, 2009). For this type of impeller most important is the space near the impeller blade, where the bubbles of dispersed gas are disintegrated only by the eddies whose size and energy are suitable to disrupt the bubble. Both parameters can be determined on the basis of local energy dissipation rate ε (Pohorecki *et al.*, 2001; Laakkonen *et al.*, 2006). This, in turn, is defined on the basis of the measurements of liquid flow velocities in the tank. Hence, to explain the phenomena occurring near the blades of a self-aspirating disk impeller an accurate hydrodynamic description in this area is required. In the case of ***PIV*** measurements the classical definition described by Eq. (1) can be used to determine the distribution of energy dissipation rates (Sharp *et al.*, 1998; Saarenrinne and Piirto, 2000; Sheng *et al.*, 2000; Baldi *et al.*, 2002; Baldi and Yianneskis, 2003;

Kilander and Rasmuson, 2005; Tanaka and Eaton, 2007; de Jong *et al.*, 2009; Delafosse *et al.*, 2011)

$$\varepsilon = \nu.\overline{\frac{\partial u_j'}{\partial x_i}\left(\frac{\partial u_i'}{\partial x_j}+\frac{\partial u_j'}{\partial x_i}\right)} = \frac{1}{2}.\nu.\overline{\left(\frac{\partial u_i'}{\partial x_j}+\frac{\partial u_j'}{\partial x_i}\right)^2} \tag{1}$$

For three-dimensional flow, where u' is the velocity pulsation in the x direction, v' is the pulsation in the y and w' in z direction, the ~~following~~ relationship (2) is obtained

$$\varepsilon = \nu.\left\{\begin{array}{l} 2.\left[\overline{\left(\frac{\partial u'}{\partial x}\right)^2}+\overline{\left(\frac{\partial v'}{\partial y}\right)^2}+\overline{\left(\frac{\partial w'}{\partial z}\right)^2}\right]+ \\ +\overline{\left(\frac{\partial u'}{\partial y}\right)^2}+\overline{\left(\frac{\partial v'}{\partial x}\right)^2}+\overline{\left(\frac{\partial u'}{\partial z}\right)^2}+ \\ +\overline{\left(\frac{\partial w'}{\partial x}\right)^2}+\overline{\left(\frac{\partial v'}{\partial z}\right)^2}+\overline{\left(\frac{\partial w'}{\partial y}\right)^2}+ \\ +2.\left(\overline{\frac{\partial u'}{\partial y}\frac{\partial v'}{\partial x}}+\overline{\frac{\partial u'}{\partial z}\frac{\partial w'}{\partial x}}+\overline{\frac{\partial v'}{\partial z}\frac{\partial w'}{\partial y}}\right) \end{array}\right\} \tag{2}$$

In the ***PIV*** method a two-dimensional velocity distribution is obtained. However, under the assumption of isotropic turbulence, the missing elements in the z direction can be replaced (Xu and Chen, 2013; Hoque *et al.*, 2015) using the ~~following~~ relationships (3), (4) and (5)

$$\overline{\left(\frac{\partial w'}{\partial z}\right)^2} = \frac{1}{2}.\left[\overline{\left(\frac{\partial u'}{\partial x}\right)^2}+\overline{\left(\frac{\partial v'}{\partial y}\right)^2}\right] \tag{3}$$

$$\overline{\left(\frac{\partial u'}{\partial z}\right)^2} = \overline{\left(\frac{\partial w'}{\partial x}\right)^2} = \overline{\left(\frac{\partial v'}{\partial z}\right)^2} = \overline{\left(\frac{\partial w'}{\partial y}\right)^2} = \frac{1}{2}.\left[\overline{\left(\frac{\partial u'}{\partial y}\right)^2}+\overline{\left(\frac{\partial v'}{\partial x}\right)^2}\right] \tag{4}$$

$$\overline{\frac{\partial u'}{\partial z}.\frac{\partial w'}{\partial x}} = \overline{\frac{\partial v'}{\partial z}.\frac{\partial w'}{\partial y}} = \frac{-\frac{1}{2}\overline{\left(\frac{\partial u'}{\partial z}\right)^2}-\frac{1}{2}\overline{\left(\frac{\partial v'}{\partial y}\right)^2}}{2} = -\frac{1}{4}.\left[\overline{\left(\frac{\partial u'}{\partial x}\right)^2}+\overline{\left(\frac{\partial v'}{\partial y}\right)^2}\right] \tag{5}$$

Upon substitutions and transformations we ~~have~~ obtain Eq. (6)

$$\varepsilon = \nu.\left[\begin{array}{c} 2.\overline{\left(\frac{\partial u'}{\partial x}\right)^2}+2.\overline{\left(\frac{\partial v'}{\partial y}\right)^2}+3.\overline{\left(\frac{\partial u'}{\partial y}\right)^2}+ \\ +3.\overline{\left(\frac{\partial v'}{\partial x}\right)^2}+2.\overline{\frac{\partial u'}{\partial y}.\frac{\partial v'}{\partial x}} \end{array}\right] \tag{6}$$

which is used to calculate local energy dissipation rates on the basis of data obtained from the two-dimensional ***PIV*** system. Literature data (Saarenrinne and Piirto, 2000) indicate, however, that Eq. (2) gives correct results with spatial resolutions (understood as distance Δl between velocity vectors in the ***PIV*** method) close to the Kolmogorov scale η_K. According to the literature (Bartels *et al.*, 2000; Micheletti *et al.*, 2004; Joshi *et al.*, 2011), good results (error of the order of 15%) in the case of $\Delta l >> \eta_K$ are obtained with filtration based on the Smagorinsky model (Rösler, 2015)

$$\varepsilon = \left(C_S.\Delta l\right)^2.\left[\frac{1}{2}.\overline{\left(\frac{\partial u_i'}{\partial x_j}+\frac{\partial u_j'}{\partial x_i}\right)^2}\right]^{3/2} \tag{7}$$

where Δl is the distance between velocity vectors in the ***PIV*** method. However, the value of ε is affected by a so-called Smagorinsky constant. Usually, $C_s = 0.17$ is assumed but there are also values ranging from 0.11 to 0.21 (Baldi *et al.*, 2002).

Often, instead of using complicated Eqs. (1-7) a simple relationship (8) combining the value of ε with velocity pulsations u' is applied

$$\varepsilon = C.\frac{\overline{u'}^3}{L} \tag{8}$$

where: $\overline{u'}$ – average velocity pulsation in terms of RMS [m/s], C – numerical coefficient, L –linear dimension [m]. According to the theory, the linear dimension L should be the size of the largest eddies in the tank (integral scale of eddies). Typically, however, it is not known and the impeller diameter is substituted for the linear dimension (Kresta and Wood, 1993) because it is assumed that the biggest eddies have dimensions similar to the impeller diameter. Such a simplification, however, requires the determination of coefficient C, which can depend additionally on rotational frequency of the impeller (for the self-aspirating disk impeller C = 5.2 (Kania and Kuncewicz, 2002) for $L = D$). The value of coefficient C was determined precisely by the method of summation of control volumes. Therefore, values calculated from Eq. (8) will be treated as reference data. Literature data (for example Micheletti *et al.*, 2004) and our own research (Stelmach *et al.*, 2005) indicate, however, that the values of ε calculated by different methods may vary considerably.

In the literature (Wilcox, 1994) one can also find a definitional relationship with the thickness of the boundary layer, but its utility for calculating ε on the basis of liquid velocity measurements seems to be limited.

Knowing the energy dissipation rate allows spatial scales of eddies to be determined (Escudié and Liné, 2003). Dimensions of the smallest eddies can be calculated from Kolmogorov's theory

$$\eta_K = \left(\frac{\nu^3}{\varepsilon}\right)^{1/4} \tag{9}$$

The size of Kolmogorov eddies also determine the size of the smallest gas bubbles that can occur in a two-phase liquid-gas system.

Another scale used to describe turbulent flows is the Taylor scale. This scale determines the size of eddies of intermediate size between the Kolmogorov η_K scale and integral scale Λ, for which fluid viscosity has a significant effect on the dynamics of the turbulent eddies in the flow. In isotropic turbulent flows, the size of eddies in this range can be

calculated from the relation (10)

$$\lambda = \sqrt{15.\nu.\frac{\overline{u'^2}}{\varepsilon}} \tag{10}$$

The largest scale in the energy spectrum is the integral scale. Eddies from this range receive energy from the impeller and transmit it to a smaller eddy (eddy cascade). The maximum size of this scale is limited by the characteristic linear dimension of the device. For Rushton turbine the sizes of eddies in this range can be calculated (Wu and Patterson, 1989) from the relation (11)

$$\Lambda = 0.85.\frac{k^{3/2}}{\varepsilon} \tag{11}$$

where $k = \frac{1}{2}\left(\overline{u'^2} + \overline{v'^2} + \overline{w'^2}\right)$ is the kinetic energy of turbulence and in the case of isotropic turbulence it is $k = \frac{3}{2}\cdot\overline{u'^2}$.Outside the impeller zone, the order of magnitude of macroscale was shown to be D/4.4 (Costes and Couderc, 1988) or D/4 (Ranade and Joshi, 1990; Michelet, 1998).

With the size of eddies their energy is connected by which they can disrupt gas bubbles flowing out of the outlets of the self-aspirating disk impeller. The wave number k corresponding to length scale r is $k = 2\cdot\pi/r$. In the previous studies (Stelmach *et al.*, 2005) it was found that for the tested impeller in the eddy energy spectrum there is an area of wave numbers in which Kolmogorov's -5/3 law (Eq. (12)) is fulfilled (inertial range)

$$E(k) = \alpha.\varepsilon^{2/3}.k^{-5/3} \tag{12}$$

where: $E(k)$ – density of eddy energy spectrum [m^3/s^2], ε – energy dissipation rate [m^2/s], k – wave number [1/m], $\alpha \approx 0.5$ – Kolmogorov's constant. Thus, if the value of ε is known, one can calculate the energy of eddy of diameter d and compare it with the surface energy of the bubble $E_s = \pi\cdot d^2\cdot\sigma$ of the same diameter.

At the beginning of self-aspiration, after exceeding the critical value of the modified number $Fr'_{cr} = 0.21$ (Forrester *et al.*, 1998; Stelmach, 2000; Ju *et al.*, 2009) the gas stream and the number of bubbles are very small, and gas bubbles only slightly interfere with the system hydrodynamics. In this case, in the analysis of phenomena occurring during gas dispersion the turbulence parameters obtained for a single-phase system can be used. For example, it has been observed for the discussed impeller that gas bubbles are broken only by eddies. Therefore, knowledge of distribution ε in the vicinity of the impeller blades should enable calculating the gas size distribution based on the population balance model. In this model, in the equations describing the frequency of bubble breaking ε is important/necessary parameter (Martinez-Bazan *et al.*, 1999; Lehr *et al.*, 2002; Laakkonen *et al.*, 2007). The first aim of the study is to examine turbulent energy dissipation rate in the vicinity of the blade of a self-aspirating disk impeller operating without gas dispersion at rotational frequency slightly higher than the critical rotational frequency. The second aim of the work is to determine the spatial turbulence scales in the tank and to analyze the energy of eddies with respect to the surface energy of gas bubbles flowing out of the impeller.

2. EXPERIMENTAL

Experiments were carried out in a flat-bottomed glass tank of diameter T = 292 mm equipped with four baffles of width $B = 0.1\cdot T$. The self-aspirating disk impeller of diameter D = 125 mm was placed at height h = 78 mm above the tank bottom. The tank was filled with distilled water (t = 20°C) to the height H = 0.3 m. Tracer particles of mean diameter 10 μm were added to water. To reduce optical distortions, a cylindrical tank was placed in a rectangular tank and the space between the walls of the tanks was filled with water. Velocity measurements were made for rotational frequency of the impeller N = 6 s^{-1} (360 min^{-1}) in the plane defined by the axis of rotation of the impeller and the bisector of the angle between the baffles (Fig. 1). In the measurement conditions the Reynolds number was Re = 93580 and the modified Froude number Fr' = 0.258. The impeller was operating without gas dispersion (the inlet in the shaft was ~~stopped~~ closed). In these conditions the power number was Po = 0.812 and the energy dissipation rate for the whole tank was ε_m = 0.266 m^2/s^3. In order to facilitate the comparison of the values of ε with other types of impellers, this parameter is often given in a dimensionless form $\varepsilon^* = \varepsilon/(D^2\cdot N^3)$. In the discussed case this is ε_m^* = 0.0788.

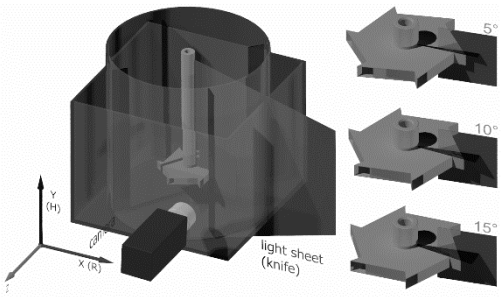

Fig. 1. Schematic diagram of the measurement system.

The measurements were made using a *LaVision* ***PIV*** measuring system with a double-pulse laser with maximum power of 135 mW and an *ImagePro* camera with 2048 px × 2048 px resolution equipped with a *Nikkor* 1.8/50 lens. The aperture of the lens was stopped down to the value ensuring a maximum resolution (the f-number was 5.6). The measurement area was approximately 60 mm × 60 mm. Laser pulses were initiated by an external trigger synchronized with impeller blade. The thickness of the light knife was 1 mm. Due to the importance of the area near the impeller blade where during a normal operation gas bubbles were subjected directly to eddies formed behind the blade, measurements were made for seven angular positions of the blade relative to the measurement plane at distances -15°, -10°, -5°, 0°, +5°, +10° and +15° in relation to the light knife (Fig. 1). For each angular position of the blade 200 double photographs were taken for velocity averaging. Time interval between the pulses was Δt = 415 μs. This value was calculated on the assumptions: 1 – radial and axial velocities are less

than 20% of tip blade velocity, 2 – pixel shift (displacement of tracer particles in the photographs) 10 pixels. The limit value for the first assumption was defined on the basis of previous measurements by the ***LDA*** method (Stelmach *et al.*, 2002).

Data processing was performed using the DaVis 7.2 program. Two-pass data processing was used with the final size of the analyzed area being 32 px × 32 px (i.e. about 0.95 mm × 0.95 mm) without overlaying.

3. RESULTS AND DISCUSSION

The spatial Kolmogorov scale calculated on the basis of mean energy dissipation rate is $\eta_K = (\nu^3/\varepsilon)^{0.25} = 0.044$ mm, while the distance between velocity vectors determined in the ***PIV*** method is many times bigger and amounts to 0.95 mm. The measurement area should have a size of 3 mm × 3 mm to ensure the distance between velocity vectors equal to the average Kolmogorov scale. Near the impeller the linear Kolmogorov scale has smaller values, thus for the adopted setting of the ***PIV*** system the flow of microstructures cannot be analyzed.

In our previous works (Stelmach *et al.*, 2003a, Stelmach *et al.*, 2003b, Kania and Kuncewicz, 2002), distribution of energy dissipation rate for random positions of the blade relative to the baffle was determined (this applies to measurements using the ***LDA*** and ***PIV*** methods). In this work, a trigger was used that was synchronized with the position of the impeller blade. Thanks to this, distribution maps of energy dissipation rate were obtained depending on the position of the measuring surface relative to the baffle.

3.1 Isotropy of Turbulence

Due to the use of the Smagorinsky model, the isotropy of turbulence for axial and radial components was investigated. In the case of isotropic turbulence the velocity pulsations in both directions should be the same. Since the measurements were made for a fixed position of the blade relative to the baffles, no periodic component was removed (Wu and Patterson, 1989; Kresta and Wood, 1993). The test results obtained using the ***LDA*** method show that beyond the impeller region the turbulence is isotropic (Stelmach, 2001). The use of the ***PIV*** method produced only two velocity components. Figures 2 and 3 show the contour plots of dimensionless mean square velocity pulsations for blade positions -15° and +15° relative to the plane of the light knife.

Analysis of these figures leads to the conclusion that outside the blade region there is nearly isotropic turbulence (for the analyzed components). The correlation coefficient between pulsation components of axial and radial velocities is $R_c = 0.705$ (the CORREL function of MS Excel was used which returns the correlation coefficient between two data sets). For data from outside the impeller region defined as $R < 70$ mm and 60 mm $< H <$ 80 mm (dashed line in Figs. 2 and 3), the correlation coefficient increases to $R_c = 0.956$. This confirms the earlier observations and justifies the possibility of averaging velocity pulsations, e.g. in the calculation of the energy dissipation rate.

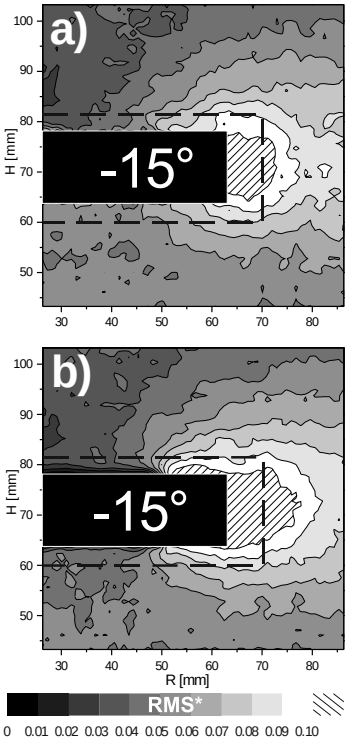

Fig. 2. Dimensionless RMS for blade 15° behind the light knife: a) radial, b) axial.

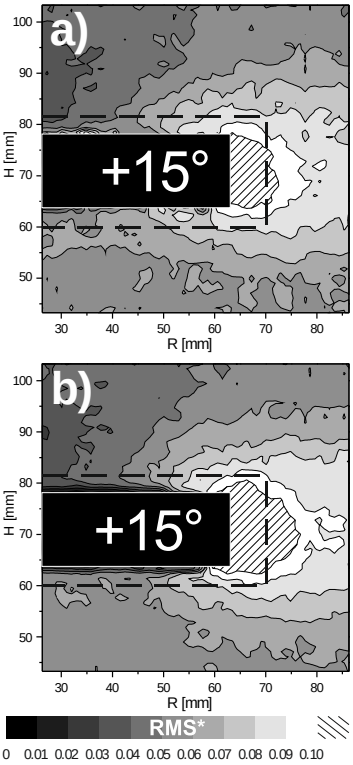

Fig. 3. Dimensionless RMS for blade 15° in front of the light knife: a) radial, b) axial.

The values of R_c for all the surveyed positions of the blade are summarized in Table 1.

Table 1 Values of correlation coefficients

Position	Correlation coefficient	
	All data	Beyond the impeller region
-15°	0.705	0.956
-10°	0.662	0.950
-5°	0.595	0.944
0°	0.721	0.943
+5°	0.595	0.944
+10°	0.673	0.944
+15°	0.649	0.946

Since the measurements for the ***PIV*** method showed isotropic turbulence for the radial and axial directions it is assumed that this is a confirmation of the results obtained by the ***LDA*** method. Previous studies have shown that there is an inertial subrange in the energy spectrum. Fulfillment of the assumption of the isotropy of turbulence makes it possible to calculate the energy dissipation rate.

3.2 Determination of the Value of Smagorinsky Constant

As mentioned previously, the value of Smagorinsky constant should be in the range from 0.11 to 0.21. Results calculated on the basis of Eq. (8) are shown in Fig. 4(a). Figure 4(b) shows the distribution of energy dissipation rates calculated from the Smagorinsky model for C_s = 0.11. The comparison of Figs. 4(a) and 4(b) leads to the conclusion that in the corresponding points of measurements there are big differences in the value of $\varepsilon^* = \varepsilon/(D^2 \cdot N^3)$ calculated from Eqs. (7) and (8). For remaining positions of the blade the results are similar.

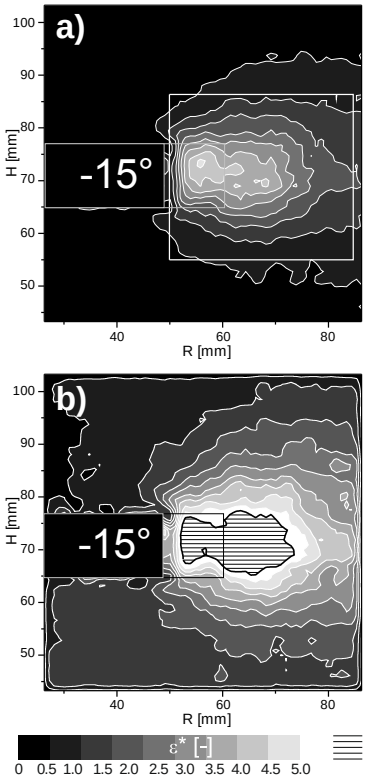

Fig. 4. Energy dissipation rate for blade 15° behind the light knife.

Because values calculated from Eq. (8) are treated as reference data, the value of Smagorinsky constant should be decreased. Figure 5(a) shows results obtained from term $\sum_i \sum_j \left(\varepsilon_{RMS_{i,j}} - \varepsilon_{S_{i,j}}\right)^2$ for different C_s values. On the other hand, Fig. 5(b) shows calculation results of the relationship $\sum_i \sum_j \varepsilon_{RMS_{i,j}} - \sum_i \sum_j \varepsilon_{S_{i,j}}$.

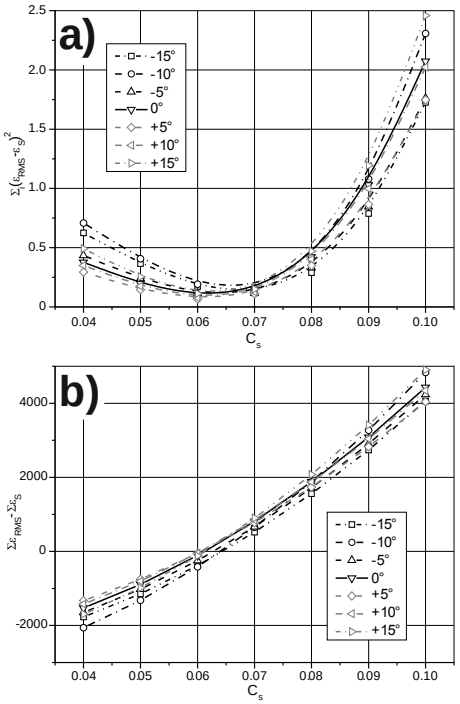

Fig. 5. Determination of the optimal value of Smagorinsky constant.

3.3 Blade 15° Behind the Light Knife

Values ε calculated from Eqs. (8) and (7) for corrected value C_s are shown in Fig. 6. Basing on Fig. 6 it can be concluded that the maximum value of ε^* occurs before the geometric center of the blade and is about 50 times bigger than the average value. A quick decrease in the value of ε^* is observed in all directions on a small area (framed in Fig. 4(a)) limited by radii R = 50 mm and R = 85 mm and heights H = 55 mm and H = 85 mm. Outside it the distribution becomes uniform. This means that in the ring near the blade most energy supplied to the tank is dissipated.

Figure 7 shows distributions of turbulence scales calculated from Eqs. (9), (10) and (11) for ε calculated from Eq. (7) at the assumed value of C_s = 0.07. To facilitate comparisons, radial profiles of turbulence scales were determined for three heights H = 60, 71 and 80 mm, i.e. for the impeller region. In this region we can find constant values of the analyzed turbulence scales. The largest eddies are about 25 mm in size which rises outside the impeller region to about 45 mm. Taylor eddies are about 0.8 mm in size which outside the impeller region slightly rises. The smallest eddies are about 0.02 mm in size,

but they are rapidly growing as they move away from the impeller region.

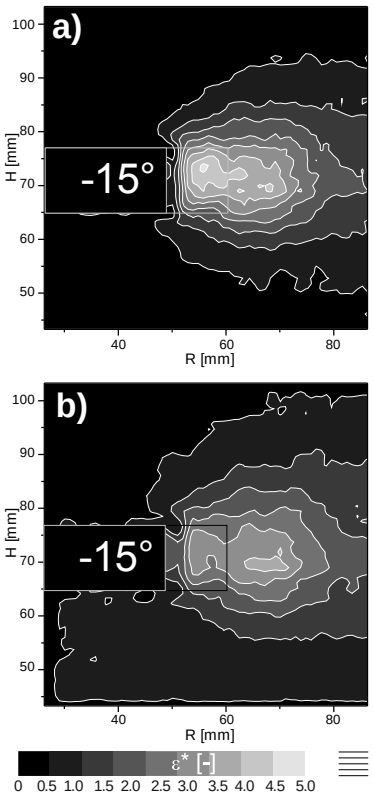

Fig. 6. Energy dissipation rate for blade 15° behind the light knife.

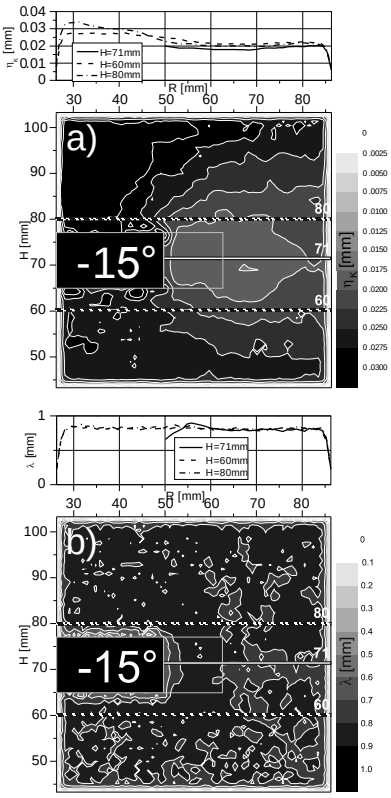

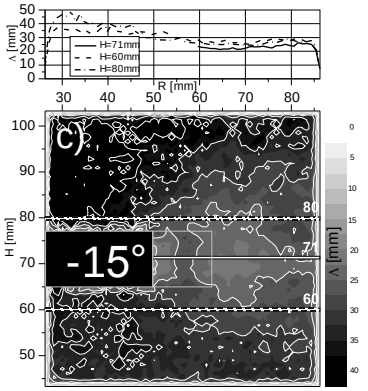

Fig. 7. Spatial turbulence scales for blade 15° behind the light knife: a) Kolmogorov's, b) Taylor's, c) integral.

3.4 Blade 10° Behind the Light Knife

For $C_s = 0.07$ distributions ε^* obtained from Eqs. (7) and (8) show good agreement (Fig. 8). The maximum values occur at the height of the impeller at a distance of about 5 mm from the impeller tip and its geometric center.

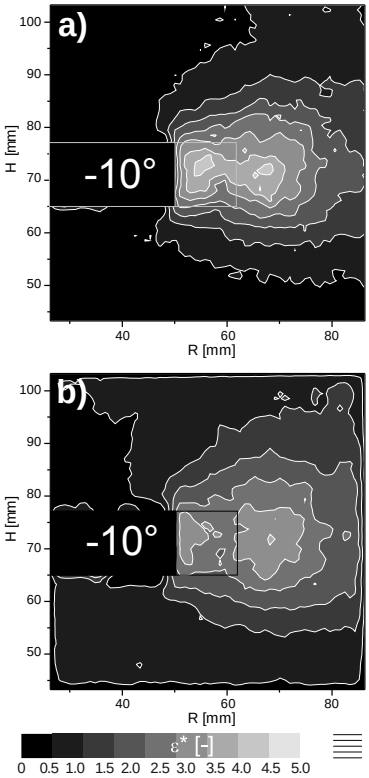

Fig. 8. Energy dissipation rate for blade 10° behind the light knife.

The turbulence scales (Fig. 9) do not change compared to the previous position of the blade.

3.5 Blade 5° Behind the Light Knife

For this blade position the distributions of energy dissipation rate did not change compared to position -10° (Fig. 10). Only their maximum values decreased slightly.

For the discussed position of the blade, no changes in turbulence scales were observed compared to positions -10° and -15° as shown in Fig. 11.

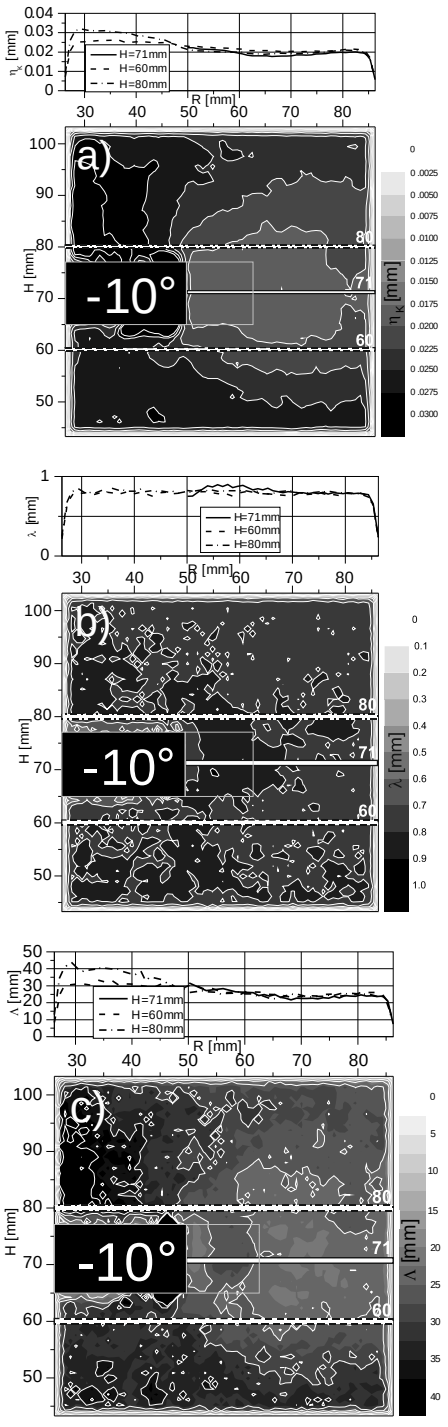

Fig. 9. Spatial turbulence scales for blade 10° behind the light knife: a) Kolmogorov's, b) Taylor's, c) integral.

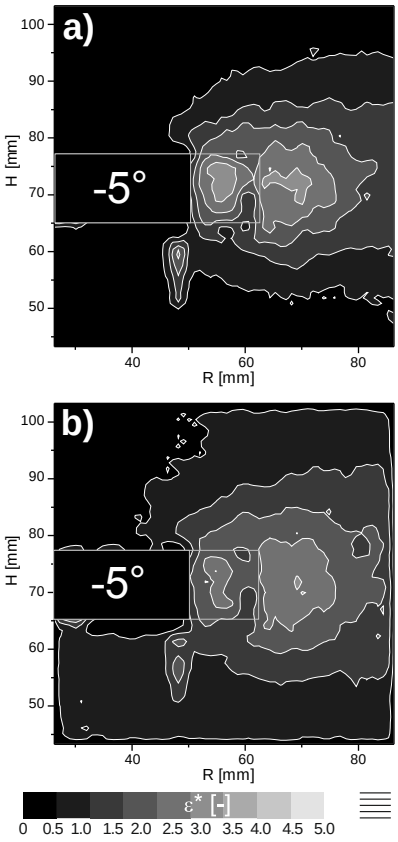

Fig. 10. Energy dissipation rate for blade 5° behind the light knife.

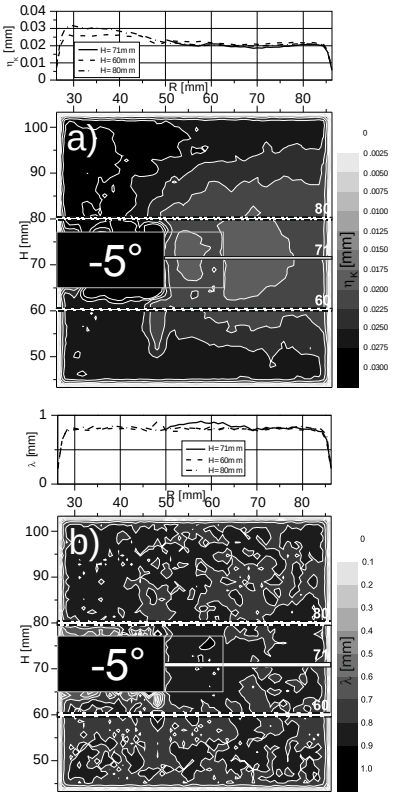

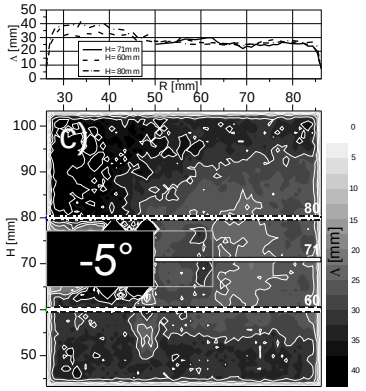

Fig. 11. Spatial turbulence scales for blade 5° behind the light knife: a) Kolmogorov's, b) Taylor's, c) integral.

3.6 Blade in the Light Knife Plane (0°)

The distributions and values of energy dissipation rates for the plane lying in the plane of the impeller blade did not change compared to position -5° (Fig. 12).

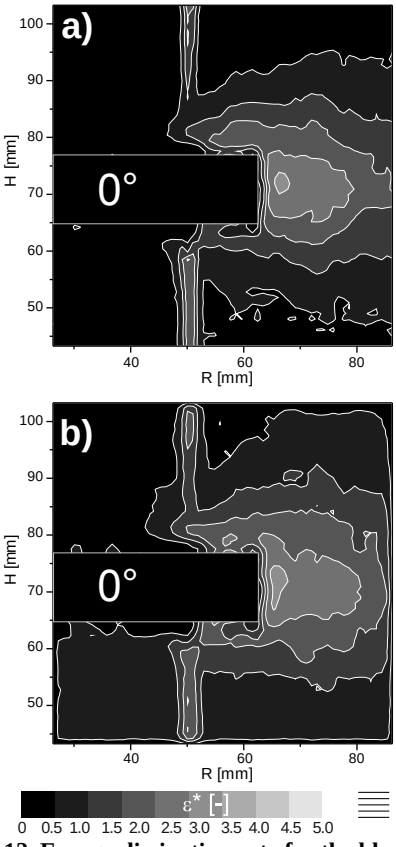

Fig. 12. Energy dissipation rate for the blade in the light knife plane.

3.7 Blade 5° in Front of the Light Knife

In the case of the distributions of energy dissipation rates (Fig. 14) the biggest values occur at a small distance from the blade tips. This means that bubbles flowing out from openings in the blade can be disrupted by eddies generated by the impeller blade.

Changing the blade position by 5° does not change the distribution of the turbulence scales (Fig. 15).

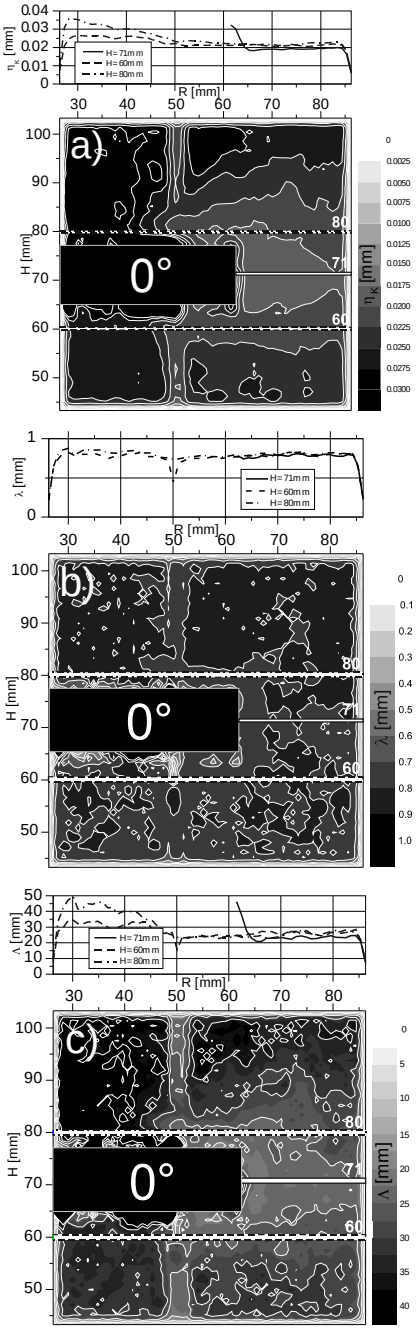

Fig. 13. Spatial turbulence scales for blade in the light knife: a) Kolmogorov's, b) Taylor's, c) integral.

3.8 Blade10° in front of the light knife

An increase of the maximum values of energy dissipation rate was observed in relation to the previous blade position. However, the area of this increase is small and its importance in the process of gas bubble disruption during gas dispersion is also small (at a small number of bubbles it is little probable that a bubble can appear in this area).

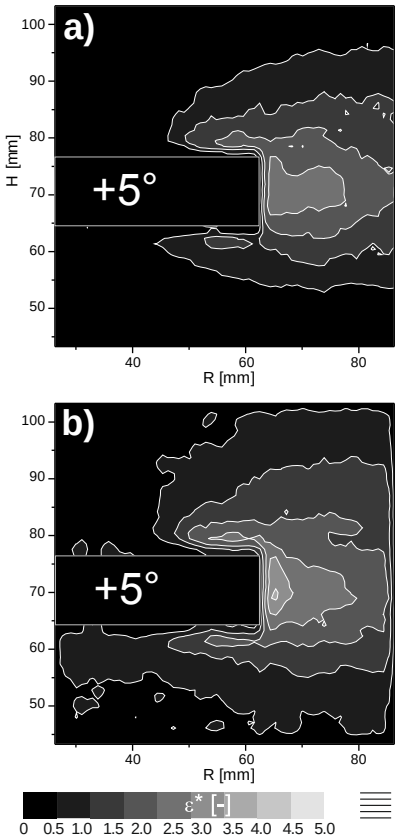

Fig. 14. Energy dissipation rate for blade 5° in front of the light knife.

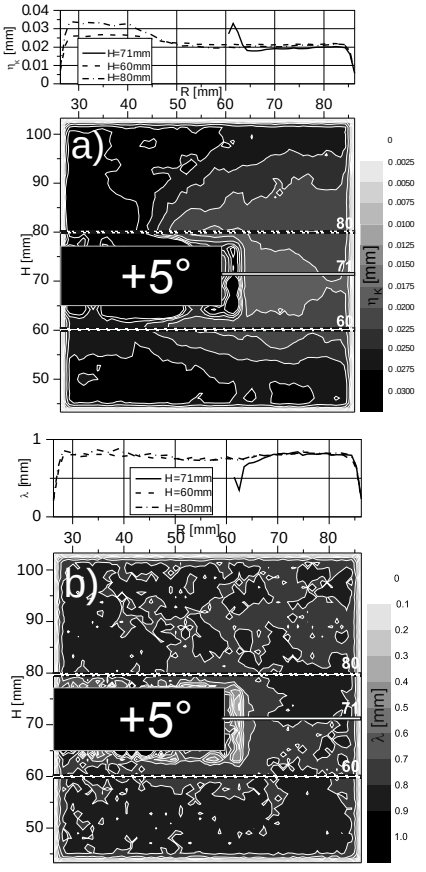

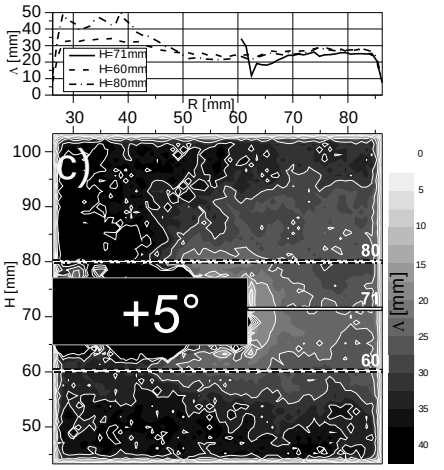

Fig. 15. Spatial turbulence scales for blade 5° in front of the light knife: a) Kolmogorov's, b) Taylor's, c) integral.

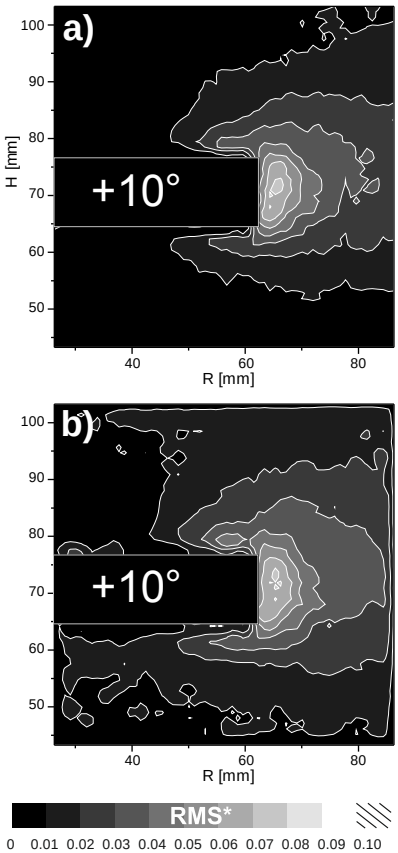

Fig. 16. Energy dissipation rate for blade 10° in front of the light knife.

Further movement of the blade does not affect the size of turbulence scales (Fig. 17).

3.9 Blade15° in Front of the Light Knife

The distribution of velocity pulsations corresponds to the distribution for position -15°.

For the last of the analyzed blade positions, the distributions of the discussed turbulence scales are almost the same as for all previous positions.

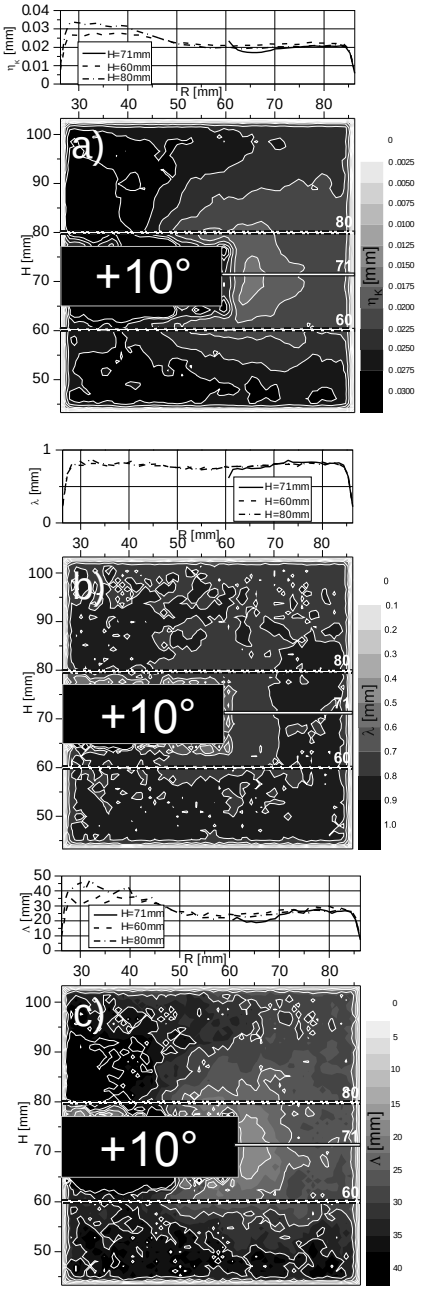

Fig. 17. Spatial turbulence scales for blade 10° in front of the light knife: a) Kolmogorov's, b) Taylor's, c) integral.

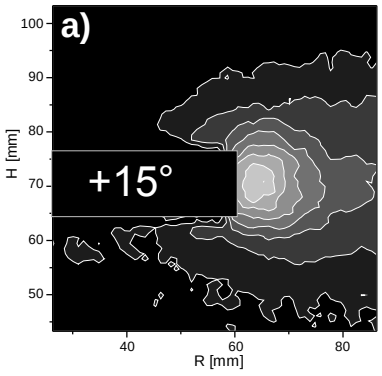

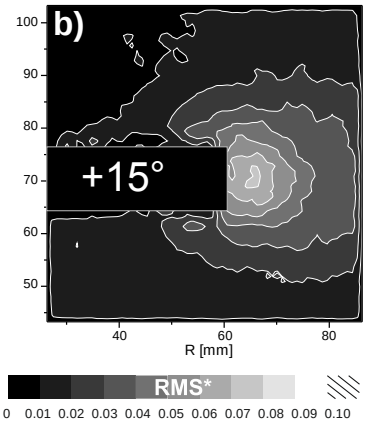

Fig. 18. Energy dissipation rate for blade 15° in front of the light knife.

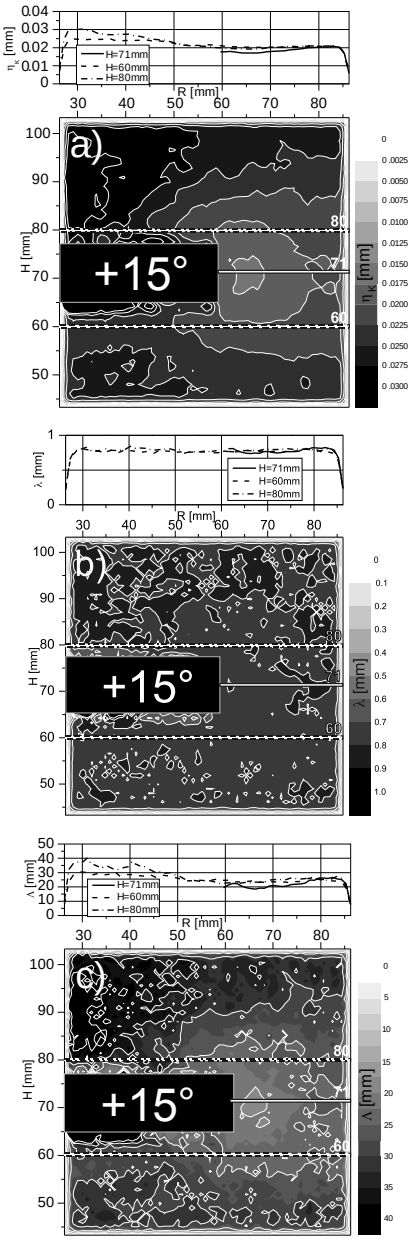

Fig. 19. Spatial turbulence scales for blade 15° in front of the light knife: a) Kolmogorov's, b) Taylor's, c) integral.

3.10 Summary and Comparison of the Self-Aspirating Disk Impeller with Rushton Turbine

The obtained results are consistent with the energy dissipation rate values obtained for the tested mixer in LDA measurements (Stelmach *et al.*, 2003a). However, the PIV method - due to the amount of data obtained in one measurement - allows for more precise determination of changes in measured parameters (for example ε) in the measurement area.

At the impeller level there is a pronounced correlation maximum value of the energy dissipation rate from the blade position relative to the baffles. The lowest values occur when the blade is in the plane between the baffles. The highest values were observed for the blade position 15° before and behind that plane. However, these changes disappear for $r/T > 0.26$, which corresponds to the radius $r \approx 75$ mm and 12.5 mm distance from the blade tip. It is a cavern space with reduced pressure (Stelmach and Musoski, 2017). Vacuum in the cavity causes the liquid to be sucked inside. The streams of liquids flowing from various directions to the caverns cause in its interior a great turbulence and strong dissipation of energy. Inside the cavern, the breaking of gas bubbles detached from the interface inside the impeller was observed.

Liquid circulation generated by the self-aspirating disk impeller is the same as the circulation for a turbine-disk impeller (Rushton turbine). The Rushton turbine is one of the most thoroughly tested impellers and is used to disperse gas supplied by a bubbler. Therefore, it can be treated as a reference impeller. Due to differences in the structure (closed and box-like construction of the self-aspirating impeller) differences can be expected in the hydrodynamics of liquid flowing in the tank. Fig. 20 shows the profiles of energy dissipation rate for the investigated impeller (Eq. (8) after smoothing) and Rushton turbine (Wu *et al.*, 1989; Micheletti *et al.*, 2004).

The maximum values for the self-aspirating disk impeller are about 4 times smaller. On the other hand, the power consumption is more than 6 times lower (Po = 0.812 for self-aspirating disk impeller (Stelmach, 2000) and Po = 5.2 for the Rushton turbine (Stręk, 1983). Probably these differences result from a larger area of blades in the Rushton turbine. This can be confirmed by changes in much higher absolute value of ε^*, which is observed particularly in the axial profile (Fig. 20(b)). It seems that for turbine impellers, measurements should be made in the same system as for a self-aspirating impeller, as according to some researches (Lee and Yianneskis, 1998; Sharp *et al.*, 1998; Sharp and Adrian, 2001; Zadghaffari *et al.*, 2010) the value of ε^* near the Rushton turbine blades reaches 20. Other researches (Delafosse *et al.*, 2009) show that the distribution of energy dissipation rates largely depends on the position of the blade relative to the measuring plane.

For the self-aspirating disk impeller the maximum dissipation rates are about 30 times bigger than the average value. Similar values are observed in the case of the Rushton turbine (Wu and Patterson, 1989; Sharp and Adrian, 2001). For both impellers the maximum dissipation rates occur at the height of the impeller. However, in the case of the Rushton turbine this occurs at a bigger radial distance from the blade tip (Sharp and Adrian, 2001). In both cases the distributions of ε^* depend on the position of blades relative to the baffles. For the Rushton turbine the highest value of ε^* is 12, while for the self-aspirating impeller it is only 4. Nevertheless, these values are many times higher than for the impellers with axial flow (Baldi *et al.*, 2002).

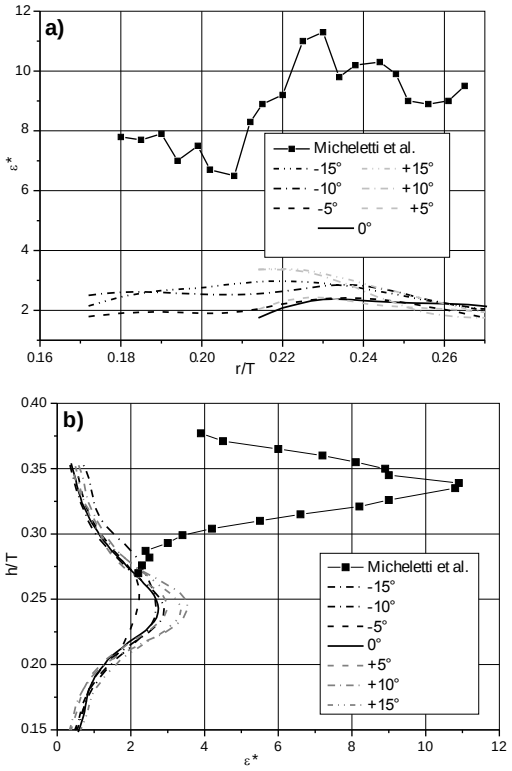

Fig. 20. Profiles of turbulent energy dissipation rate.

The energy dissipation rate affects the turbulence scales. At the height of the Rushton impeller, the integral turbulence scale Λ is about 1 mm (Lee and Yianneskis, 1998), while for the self-aspirating impeller it is several times larger reaching about 25 mm. However, for the Rushton turbine some authors (Ståhl Wernersson and Trägårdh, 2000) give also bigger, close to 50 mm, values of this scale.

Near the impeller, the Kolmogorov length scale is approximately 0.02 mm. At the same time, it is the lower limit of the size of the gas bubbles dispersed by the test impeller.

Eddies of the Taylor scale have approximately 0.8 mm near the impeller tip. Therefore, they are smaller than the Sauter diameter d_{32} = 1.59 mm gas bubbles at the rotational frequency N = 6 s^{-1} (Stelmach, 2007).

At the impeller level, the dimensions of the integral

eddy scale are about 25 mm, i.e. they are several times smaller than the diameter of the impeller. This means that the use of the impeller diameter as a linear dimension in Eq. (8) is not entirely justified. However, it should be remembered that the dimensions of eddies with an integral scale are not known a priori. The linear dimension used only affects the value of the coefficient in Eq. (8). Since this value is determined experimentally for a given type of impeller, the use of the impeller diameter as a linear dimension does not lead to incorrect values of ε.

In the area marked in Fig. 4(a) – the most important from the point of view of the ability of eddies to break bubbles – changes in turbulence scales are small and do not exceed several percent.

3.11 Ability to Break up Bubbles

Gas bubbles flowing out from the outlets of the self-aspirating disk impeller are disrupted by eddies generated by the impeller. Figure 21 shows energy of the eddies of size ranging from d = 0.01 mm to d = 30 mm calculated from Eq. (25) for ε^* = 4.5. In the same figure and for the same range of diameters, the surface energy of bubbles determined by equation $E_s = \pi \cdot d^2 \cdot \sigma$ is also shown.

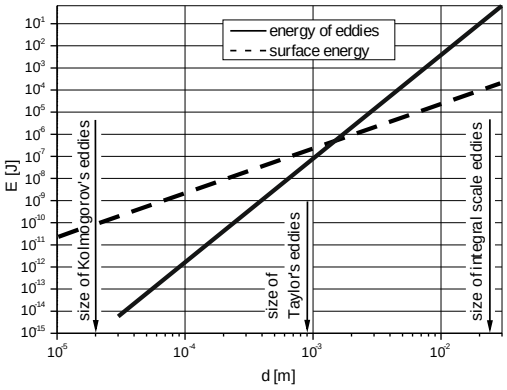

Fig. 21. Comparison of the energy of eddies and bubbles.

In order for the eddy to disrupt a gas bubble its energy must be greater than the surface energy of the bubble (the bursting force must be greater than the cohesive force). More importantly, the size of the eddy should be smaller than that of the broken bubble (Lehr *et al.*, 2002, Martín *et al.*, 2008). For the assumed value of ε eddies greater than 1.5 mm meet this condition. According to Stelmach *et al.* (2016) the sizes of bubbles flowing out of the impeller are less than 10 mm. Thus, for the self-aspirating disk impeller eddies behind the blade can disrupt gas bubbles in a fairly large range of their diameters. On the other hand, the observed presence of gas bubbles smaller than 1.5 mm can be explained in two ways:

1. instantaneous energy dissipation rates may well exceed the average value accepted for calculation,
2. small bubbles can form when disrupting larger bubbles.

5. CONCLUSIONS

Calculations of the energy dissipation rate based on the dimensional equation and Smagorinsky model give similar results, but correction of the Smagorinsky constant is necessary. High values of the energy dissipation rate appear also in the ring of inner radius 50 mm, external radius 85 mm and bases distant by 10 mm from horizontal surfaces of the impeller, i.e. slightly bigger than in the case of velocity. In this annular space most energy supplied by the impeller is dissipated. The small size of this space is most probably due to the small blade surface as compared to the Rushton turbine.

In the space close to the impeller the average eddy size from the Kolmogorov (dissipative) range is η = 0.02 mm. The average size of eddies in the Taylor scale is λ = 0.85 mm, and for the integral scale this value is Λ = 25 mm. Outside of the impeller region these values increase.

Eddies generated by the self-aspirating disk impeller have energy sufficient to disrupt gas bubbles flowing out from the outlets.

The maximum values of the dimensionless energy dissipation rate for the Rushton turbine are approximately 3 times greater than for the self-aspirating impeller, while the mixing power is more than 6 times greater. This means that blades with smaller surfaces can also effectively transfer energy to the liquid.

ACKNOWLEDGEMENTS

The study was carried out within project no. 501/10-34-1-7217

REFERENCES

Baldi, S. and M. Yianneskis (2003). On the direct measurement of turbulence energy dissipation in stirred vessels with PIV. *Industrial Engineering and Chemical Research* 42, 7006-7016.

Baldi, S., D. Hann and M. Yianneskis (2002). On the measurements of turbulence energy dissipation in stirred vessels with PIV techniques. *Proceedings of the 10th International Symposium on Applications of Laser Techniques to Fluid Mechanics*, Lisbon, Portugal.

Bartels, C., M. Breuer and F. Durst (2000). Comparison between Direct Numerical Simulation and k-ε prediction of the flow in vessel stirred by a Rushton turbine. *Proceedings of the 10th European Conference on Mixing*, 239-246, Delft, the Netherlands.

Costes, J. and J.P. Couderc (1988). Study by laser Doppler anemometry of turbulent flow induced by a Rushton turbine in a stirred tank: Influence of the Size of the Units: I. Mean Flow and Turbulence. *Chemical Engineering Science* 43, 2751-2764.

De Jong, J., L. Cao, S.H. Woodward, J.P.L.C. Salazar, L.R. Collins and H. Meng (2009). Dissipation rate estimation from PIV in zero-mean isotropic turbulence. *Experiments in Fluids* 46, 499-515.

Delafosse, A., J. Morchain, P. Guiraud and A. Line (2009). Trailing vortices generated by a Rushton turbine: Assessment of URANS and large eddy simulations. *Chemical Engineering Research and Design* 87, 401-411.

Delafosse, A., M. L. Collignon, M. Crine and D. Toye (2011). Estimation of the turbulent kinetic energy dissipation rate from 2D-PIV measurements in a vessel stirred by an axial Mixel TTP impeller. *Chemical Engineering Science* 66, 1728-1737.

Escudié, R. and A. Liné (2003). Experimental analysis of hydrodynamics in a radially agitated tank. *AIChE Journal* 49, 585-603.

Forrester, S.E., C.D. Rielly and K.J. Carpenter (1998). Gas-inducing impeller design and performance characteristics. *Chemical Engineering Science* 55, 603-615.

Hoque, M. M., M. J. Sathe, S. Mitra and J. B. Joshi (2015). Comparison of specific energy dissipation rate calculation methodologies utilizing 2D PIV velocity measurement. *Chemical Engineering Science* 137, 752-767.

Joshi, J. B., N. K. Nere, C. V. Rane, B. N. Murthy, C. S. Mathpati, A. W. Patwardhan and V. V. Ranade (2011). CDF simulation of stirred tanks: Comparison of turbulence models. Part I: Radial flow impellers. *Canadian Journal of Chemical Engineering* 89, 23-82.

Kania, A. and Cz. Kuncewicz (2002). Energy dissipation rate and the size of eddies in the tank with self-aspirating impeller. *Proceedings of the 15th International Congress of Chemical & Process Engineering CHISA*, Prague, Czech Republic.

Kilander, J. and A. Rasmuson (2005). Energy dissipation and macro instabilities in a stirred square tank investigated using an LE PIV approach and LDA measurements. *Chemical Engineering Science* 60, 6844-6856.

Kresta, S.M. and P.E. Wood (1993). The flow field produced by a pitched blade turbine: Characterization of the turbulence and estimation of the dissipation rate. *Chemical Engineering Science* 48(10), 1761-1774.

Kurasiński, T. and Cz. Kuncewicz (2009). Liquid circulation in a mixer and its influence on mass transfer in the gas-liquid system. *Inżynieria i Aparatura Chemiczna* 4, 48(40), 75-76. (in Polish)

Laakkonen, M., P. Moilanen, V. Alopaeus and J. Aittamaa (2006). Modelling local gas-liquid mass transfer in agitated vessels. *Proceedings of the 12th European Conference on Mixing*, Bologna, Italy.

Laakkonen, M., P. Moilanen, V. Alopaeus and J. Aittamaa (2007). Modeling local bubble size distribution in agitated vessels. *Chemical Engineering Science*, 62, 721-740.

Lee, K. C. and M. Yianneskis (1998). Turbulence properties of the impeller stream of a Rushton turbine. *AIChE Journal* 44, 13-24.

Lehr, F., M. Millies and D. Mewes (2002). Bubble-size distributions and flow fields in bubble columns. *AIChE Journal, Fluids Mechanics and Transport Phenomena* 48, 2426-2443.

Martín, M., F. J. Montes and M.A. Galán (2008). Influence of impeller type on the bubble breakup process in stirred tanks. *Industrial Engineering and Chemical Research* 47, 6251-6263.

Martinez-Bazán C., J. L. Montañés and J.C. Lasheras (1999). On the breakup of an air bubble injected into a fully developed turbulent flow. Part 1. Breakup frequency. *Journal of Fluid Mechanics*, 401, 183-207.

Michelet, S. (1998). Turbulence et Dissipation au Sein d'un Réacteur Agité par une Turbine Rushton – Vélocimétrie Laser Doppler à Deux Volumes de Mesure, Ph. D. thesis, l'Institut National Polytechnique de Lorraine, Nancy, France.

Micheletti, M., S. Baldi, S. L. Yeoh, A. Ducci, G. Papadakis, K.C. Lee and M. Yanneskis (2004). On spatial and temporal variations and estimates of energy dissipation in stirred reactors. *Chemical Engineering Research and Design* 82, 1188-1198.

Pohorecki, R., W. Moniuk, P. Bielski and A. Zdrójkowski (2001). Modeling of the coalescence/redispersion processes in bubble columns. *Chemical Engineering Science* 56, 6157-6164.

Ranade, V. R. and V. Joshi (1990). Flow Generated by a Disc Turbine: Part I: *Experimental. Chemical Engineering Research and Design* 68, 19-33.

Rösler, M. (2015). The Smagorinsky turbulence model, Bachelor thesis at the Institute of Mathematics of Freie Universität Berlin, Germany.

Saarenrinne, P. and M. Piirto (2000). Turbulent kinetic energy dissipation rate estimation from PIV vector fields. *Experiments in Fluids* [Supplement], S300-S307.

Sharp, K.V. and R.J. Adrian (2001). PIV study of small-scale flow structure around a Rushton turbine. *AIChE Journal* 47, 766-777.

Sharp, K.V., K.C. Kim and R. Adrian (1998). Dissipation estimation around a Rushton turbine using particle image velocimetry. *Proceedings of the 9th International Symposium on Applications of Laser Techniques to Fluid Mechanics*, Lisbon, Portugal.

Sheng, J., H. Meng and R.O. Fox (2000). A large eddy PIV method for turbulence dissipation rate estimation. *Chemical Engineering Science* 55, 4423-4434.

Ståhl Wernersson, E. and C. Trägårdh (2000). Measurements and analysis of high-intensity turbulent characteristics in a turbine-agitated tank. *Experiments in Fluids* 28, 532-545.

Stelmach, J. (2000). Investigation of self-aspirating disk impeller work. *PhD thesis*, Lodz University of Technology, Łódź. (in Polish)

Stelmach, J. (2001). Velocity fluctuations at the height of the self-aspirating disk impeller. *Chemical and Process Engineering* 22(3e), 1315-1320. (in Polish)

Stelmach, J. (2007). Distribution of gas bubble sizes at the beginning of self-aspirating. *Inżynieria i Aparatura Chemiczna* 4-5, 117-119. (in Polish)

Stelmach, J. and R. Musoski (2017). Hydrodynamics in the blade region of a self-aspirating disk impeller. *Journal of Applied Fluid Mechanics* 10, 1177-1188.

Stelmach, J., Cz. Kuncewicz and R. Musoski (2016). Analysis of the mechanism of gas bubbles break-up in liquids during the self-aspirating impeller operation. *Chemical and Process Engineering* 37, 441-457.

Stelmach, J., E. Rzyski and A. Kania (2003a). Energy dissipation on the level of a self-aspirating disk impeller, *Proceedings of the 11th European Conference on Mixing*, Bamberg, Germany.

Stelmach, J., E. Rzyski and F. Rieger (2003b). Energy dissipation rate for disk impeller. *Inżynieria I Aparatura Chemiczna* 42, 143-144.

Stelmach, J., T. Kurasiński and Cz. Kuncewicz (2005). Comparative analysis of selected methods for calculation of energy dissipation rate. *Chemical and Process Engineering* 26, 201-215 (in Polish)

Stręk, F. (1983). *Mieszanie i mieszalniki*. WNT, Warsaw, Poland. (in Polish)

Tanaka, T. and J.K. Eaton (2007). A correction method for measuring turbulence kinetic energy dissipation rate by PIV. *Experiments in Fluids* 42, 893-902.

Wilcox, D.C. (1994) Turbulence modeling for CFD, DCW Industries.

Wu, H. and G. K. Patterson (1989). Laser-Doppler measurements of turbulent-flow parameters in a stirred mixer. *Chemical Engineering Science* 44, 2207-2221.

Wu, H., G. K. Patterson and M. Van Dorn (1989). Distribution of turbulence energy dissipation rates in a Rushton turbine stirred mixer. *Experiments in Fluids* 8, 153-160.

Xu, D. and J. Chen (2013). Accurate estimate of turbulent dissipation rate using PIV data. *Experimental Thermal and Fluid Science* 44, 662-672.

Zadghaffari, R., J. S. Moghaddas and J. Revstedt (2010). Large-eddy simulation of turbulent flow in a stirred tank driven by a Rushton turbine. *Computers and Fluids* 39, 1183-1190.

Ju, F., Z. M. Cheng, J. H. Chen, X. H. Chu, Z. M. Zhou and P. Q. Yuan (2009). A novel design for a gas-inducing impeller at the lowest critical speed. *Chemical Engineering Research and Design* 87, 1069-1074.

Stelmach, J. and E. Rzyski (2002). LDA measurement in the impeller region of stirred vessels: an assessment of measurement technique, *Chem. Biochem. Eng. Q.*,16, 173-177.